Chronic innate immune activation of TBK1 suppresses mTORC1 activity and dysregulates cellular metabolism

Maroof Hasan[a,1,2], Vijay K. Gonugunta[a,1], Nicole Dobbs[a], Aktar Ali[b], Guillermo Palchik[c], Maria A. Calvaruso[d], Ralph J. DeBerardinis[d,e,f], and Nan Yan[a,g,3]

[a]Department of Immunology, University of Texas Southwestern Medical Center, Dallas, TX 75390; [b]Department of Internal Medicine, University of Texas Southwestern Medical Center, Dallas, TX 75390; [c]Department of Radiation Oncology, University of Texas Southwestern Medical Center, Dallas, TX 75390; [d]Children's Medical Center Research Institute, University of Texas Southwestern Medical Center, Dallas, TX 75390; [e]Department of Pediatrics, University of Texas Southwestern Medical Center, Dallas, TX 75390; [f]McDermott Center for Human Growth and Development, University of Texas Southwestern Medical Center, Dallas, TX 75390; and [g]Department of Microbiology, University of Texas Southwestern Medical Center, Dallas, TX 75390

Edited by Michael Karin, University of California, San Diego School of Medicine, La Jolla, CA, and approved December 9, 2016 (received for review July 7, 2016)

Three-prime repair exonuclease 1 knockout (*Trex1*$^{-/-}$) mice suffer from systemic inflammation caused largely by chronic activation of the cyclic GMP-AMP synthase–stimulator of interferon genes–TANK-binding kinase–interferon regulatory factor 3 (cGAS–STING–TBK1–IRF3) signaling pathway. We showed previously that *Trex1*-deficient cells have reduced mammalian target of rapamycin complex 1 (mTORC1) activity, although the underlying mechanism is unclear. Here, we performed detailed metabolic analysis in *Trex1*$^{-/-}$ mice and cells that revealed both cellular and systemic metabolic defects, including reduced mitochondrial respiration and increased glycolysis, energy expenditure, and fat metabolism. We also genetically separated the inflammatory and metabolic phenotypes by showing that *Sting* deficiency rescued both inflammatory and metabolic phenotypes, whereas *Irf3* deficiency only rescued inflammation on the *Trex1*$^{-/-}$ background, and many metabolic defects persist in *Trex1*$^{-/-}$*Irf3*$^{-/-}$ cells and mice. We also showed that *Leptin* deficiency (*ob*/*ob*) increased lipogenesis and prolonged survival of *Trex1*$^{-/-}$ mice without dampening inflammation. Mechanistically, we identified TBK1 as a key regulator of mTORC1 activity in *Trex1*$^{-/-}$ cells. Together, our data demonstrate that chronic innate immune activation of TBK1 suppresses mTORC1 activity, leading to dysregulated cellular metabolism.

TREX1 | TBK1 | mTORC1 | innate immunity | metabolism

Mammals have evolved complex and integrated systems of immunity and metabolism to maintain and defend internal and environmental threats. Increasing numbers of immune regulators have been found to play critical roles in metabolism. Studies from recent years have established an integrated view on the shared architecture between adaptive immunity and metabolism, including how they correspond to stimulus in disease settings. However, cell-intrinsic innate immune regulation of metabolic pathways remains poorly understood. This is in part due to the fact that overwhelming systemic inflammation in chronic diseases often masks direct underlying molecular causes.

We have previously characterized an autoimmune/autoinflammatory disease mouse model, three-prime repair exonuclease 1 knockout (*Trex1*$^{-/-}$) (1). TREX1, also known as DNase III, is an exonuclease that localizes to the endoplasmic reticulum (ER) to prevent aberrant accumulation of self-DNA or glycans that would trigger immune activation (2, 3). Mutations of the *TREX1* gene have been associated with several autoinflammatory and autoimmune diseases, including Aicardi–Goutières syndrome and systemic lupus erythematosus (SLE) (4). *Trex1*$^{-/-}$ mice suffer from systemic inflammation caused largely by chronic activation of the cytosolic DNA sensing pathway through the cyclic GMP-AMP synthase–stimulator of interferon genes–TANK-binding kinase–interferon regulatory factor 3 (cGAS–STING–TBK1–IRF3) cascade (5–7). We showed previously that TREX1 also regulates lysosomal biogenesis through the mTORC1–TFEB pathway and that *Trex1*$^{-/-}$ mouse embryonic fibroblasts (MEFs) exhibit drastically reduced mTORC1 activity compared with WT cells (1). The molecular mechanism leading to suppression of mTORC1 activity remains unknown.

Here, we show that mTORC1 activity is reduced in multiple *Trex1*$^{-/-}$ mouse tissues and *TREX1* mutant human cells. We also show that *Trex1*$^{-/-}$ mice exhibit many metabolic-dysregulation phenotypes consistent with chronically reduced mTORC1 activity, including reduced cellular mitochondrial respiration and increased in vivo energy expenditure and fat metabolism, leading to reduced adiposity and survival. We genetically separated inflammation and metabolic defects and demonstrate that metabolic dysregulation in *Trex1*$^{-/-}$ mice is caused by innate immune activation of TBK1, but not the downstream IRF3 signaling and inflammation, and that TBK1 binds to the mTORC1 complex and inhibits its activity in *Trex1*$^{-/-}$ cells. Our data thus establish TBK1–mTORC1 as an important regulatory axis between cell-intrinsic immune signaling and metabolism.

Results

Reduced mTORC1 Activity and Cellular Metabolism in *Trex1*$^{-/-}$ Cells and Tissues. Recently, we showed that *Trex1*$^{-/-}$ cells have reduced mTORC1 activity, but the underlying mechanism is unclear (1). *Trex1*$^{-/-}$ mice also display reduced body size and weight that resembles reduced mTORC1 function as in *S6K*$^{-/-}$ or *Raptor* conditional knockout mice (8, 9) (Fig. 1*A*). To extend our earlier in vitro findings, we first evaluated the mTORC1 activity in tissues of *Trex1*$^{-/-}$ mice. We observed clear reduction in mTORC1 activity (measured by S6P and 4EBP phosphorylation) in the liver, skeletal muscles, and kidney of *Trex1*$^{-/-}$ mice (Fig. 1*B* and

Significance

Patients with chronic autoimmune and autoinflammatory diseases often also present metabolic phenotypes. The molecular connection between inflammation and metabolism is incompletely understood. We describe a mouse model, three-prime repair exonuclease 1 knockout, that presents both chronic systemic inflammation and metabolic dysregulation. We genetically separated the inflammation and metabolic phenotypes and biochemically identified TANK-binding kinase 1 (TBK1) as a key regulator of mammalian target of rapamycin complex 1, a master regulator of metabolism. Chronically activated TBK1 and interferon signaling are associated with many autoimmune diseases, including systemic lupus erythematosus. Our study provides a mechanism by which the innate immune signaling pathways regulate cellular metabolism.

Author contributions: M.H., V.K.G., and N.Y. designed research; M.H., V.K.G., N.D., A.A., G.P., and M.A.C. performed research; A.A. and R.J.D. contributed new reagents/analytic tools; M.H., V.K.G., N.D., G.P., M.A.C., and N.Y. analyzed data; and M.H., V.K.G., and N.Y. wrote the paper.

The authors declare no conflict of interest.

This article is a PNAS Direct Submission.

[1]M.H. and V.K.G. contributed equally to this work.

[2]Present address: Novartis Institutes of BioMedical Research, Basel, Switzerland.

[3]To whom correspondence should be addressed. Email: nan.yan@utsouthwestern.edu.

This article contains supporting information online at www.pnas.org/lookup/suppl/doi:10.1073/pnas.1611113114/-/DCSupplemental.

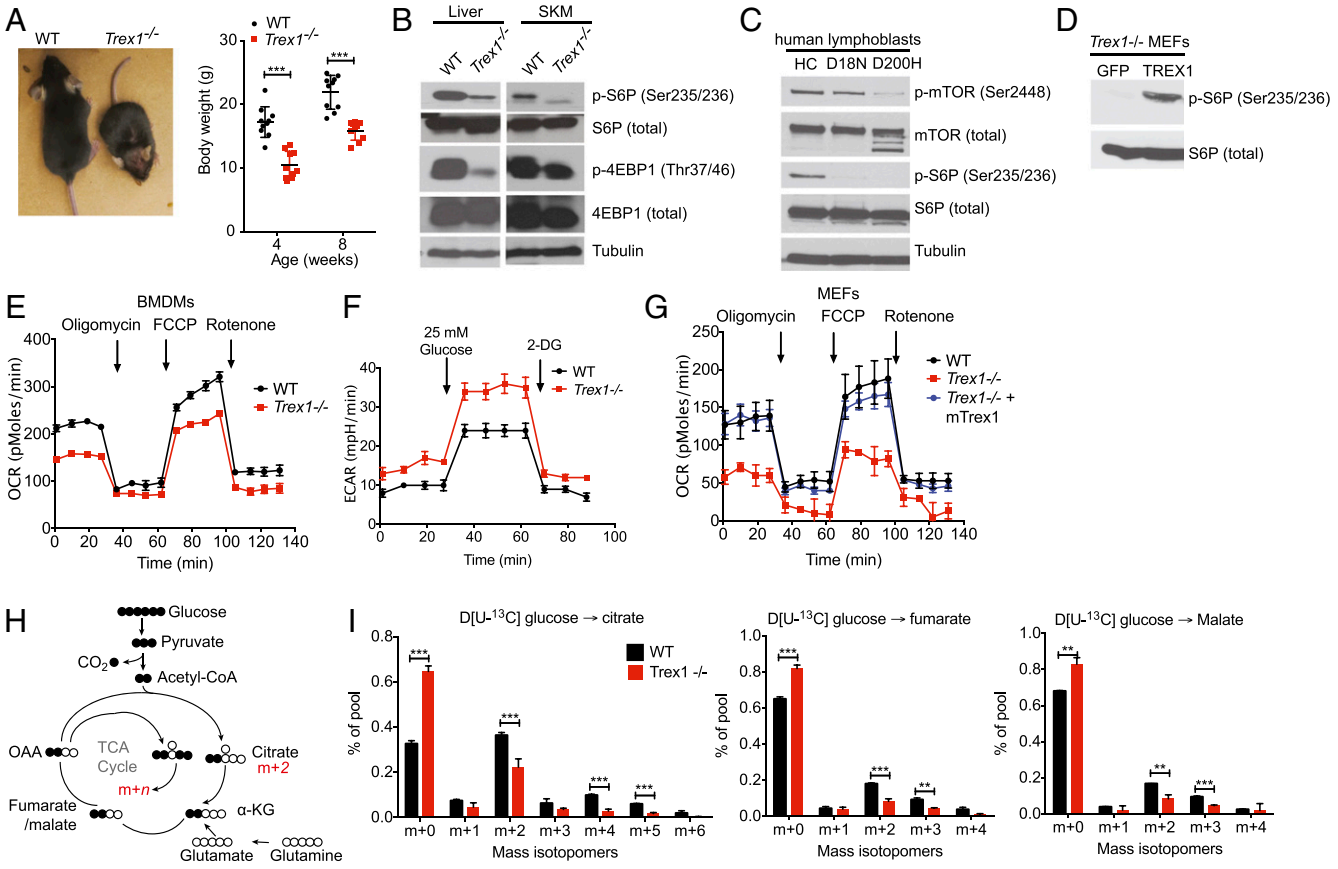

Fig. 1. Reduced mTORC1 activity and defective mitochondrial respiration in *Trex1*$^{-/-}$ cells and tissues. (*A*) Representative images of WT and *Trex1*$^{-/-}$ mice at the age of 6–8 wk. Body weight was measured at 8 wk (n = 10). (*B*) Immunoblot analysis of phosphorylated and total S6P and 4E-BP1 in WT and *Trex1*$^{-/-}$ mouse tissues. (*C*) Immunoblot analysis of phosphorylated and total mTOR and S6P in healthy control (HC) and *TREX1-D18N* and *TREX1-D200H* mutant patient lymphoblasts. (*D*) Immunoblot analysis of phosphorylated and total S6P in *Trex1*$^{-/-}$ MEFs reconstituted with GFP (control) or mouse TREX1. (*E–G*) Real-time changes in the OCR and ECAR of WT or *Trex1*$^{-/-}$ BMDMs (*E* and *F*) or MEFs (*G*). OCR was assessed during subsequent sequential treatment with oligomycin (inhibitor of ATP synthase), FCCP (carbonyl cyanide 4-(trifluoromethoxy) phenylhydrazone), and rotenone (inhibitors of the electron-transport chain). ECAR was assessed during sequential treatment with 25 mM glucose and 2-deoxyglucose (2-DG). (*H*) Schematic representation of metabolism of [U-^{13}C]glucose for experiments in *G*. (*I*) Mass isotopomer analysis of citrate, fumarate, and malate in cells cultured with [U-^{13}C]glucose and unlabeled glutamine. Data are presented as the means ± SEM of quadruplets of two to three independent experiments. *P < 0.05; **P < 0.01; ***P < 0.001 (Student's t test).

Fig. S1 *A* and *B*). Interestingly, AKT phosphorylation is unchanged in *Trex1*$^{-/-}$ tissues where mTORC1 activity is clearly reduced, indicating that mTORC1 is regulated independent of AKT in these tissues (Fig. S1*B*). We observed some reduction of 4E–BP phosphorylation in *Trex1*$^{-/-}$ bone marrow-derived dendritic cells (BMDCs), and in adipose tissue, we observed both reduced mTORC1 activity and AKT phosphorylation (Fig. S1 *C* and *D*). We also measured mTORC1 activity in *TREX1* mutant human patient lymphoblasts. Both D18N and D200H mutations disrupt TREX1 DNase activity and activate DNA-mediated innate immune activation. We observed reduced mTORC1 activity in both TREX1 mutant human patient cells (Fig. 1*C*).

We next asked whether reexpressing TREX1 can restore mTORC1 activity in *Trex1*$^{-/-}$ cells. We stably reconstituted *Trex1*$^{-/-}$ MEFs with retroviral constructs expressing WT mouse TREX1, which restored mTORC1 activity (Fig. 1*D*), suggesting that lack of TREX1 protein or subsequent immune signaling pathways activated by *Trex1* deficiency are responsible for mTORC1 suppression.

mTORC1 is known to regulate mitochondrial function (10). To explore whether the chronic suppression of mTORC1 activity in *Trex1*$^{-/-}$ cells is associated with defects in cellular metabolism, we analyzed the oxygen consumption rate (OCR), which is an indicator of mitochondrial respiration. Indeed, we observed drastically reduced mitochondrial respiration in *Trex1*$^{-/-}$ MEFs and bone marrow-derived macrophages (BMDMs) compared with WT cells (Fig. 1*E*). We also observed increased glycolysis in *Trex1*$^{-/-}$ cells measured by extracellular acidification rate (ECAR) (Fig. 1*F*). The mitochondrial-respiration defect in *Trex1*$^{-/-}$ MEFs was completely restored by reexpressing WT TREX1 (Fig. 1*G*). To confirm the mitochondrial defect and pinpoint the specific step(s) of cellular metabolism that might be affected by *Trex1*$^{-/-}$, we performed ^{13}C isotope tracing to determine the fate of glucose-derived carbon (11). After culturing with [U-^{13}C]glucose, the unlabeled fraction of citrate (m+0) was significantly increased in *Trex1*$^{-/-}$ cells compared with WT, whereas the fraction of labeled citrate arising from ^{13}C entry into and progression around the TCA cycle (m+2, m+4, and m+5) was significantly decreased (Fig. 1 *H* and *I*). Together, these data suggest that reduced mitochondrial respiration observed in *Trex1*$^{-/-}$ cells is likely caused by a defect in the delivery of glucose-derived carbon to the mitochondria for oxidation.

Cellular Metabolic Defect Associated with *Trex1* Deficiency Is Dependent on STING but Independent of IRF3 and Inflammation. *Trex1*$^{-/-}$ mice succumb to systemic inflammation early in age, largely due to immune activation by self-DNA through the cGAS–STING–TBK1–IRF3 pathway (6, 7). Upon activation by DNA, cGAS produces cyclic GMP–AMP (cGAMP) dinucleotide that activates STING on the ER. STING then moves from the ER to cytoplasmic vesicles through the secretory pathway, during which time STING recruits protein kinase TBK1, which phosphorylates itself, STING, and transcription factor IRF3, leading to activation of IFN genes. Both *Sting* and *Irf3* deficiency rescue inflammation

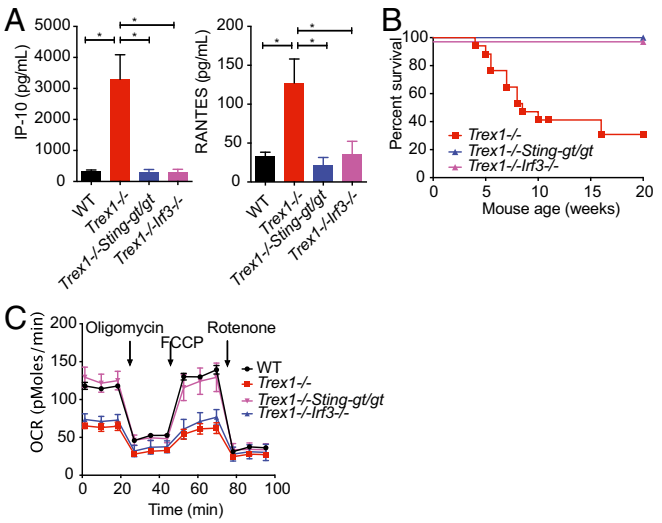

Fig. 2. Cellular metabolic defect associated with *Trex1*$^{-/-}$ is STING-dependent but IRF3-independent. (*A*) Serum levels of indicated inflammatory cytokines in WT, *Trex1*$^{-/-}$, *Trex1*$^{-/-}$*Sting*$^{gt/gt}$, and *Trex1*$^{-/-}$*Irf3*$^{-/-}$ mice. (*B*) Survival curve of *Trex1*$^{-/-}$, *Trex1*$^{-/-}$*Sting*$^{gt/gt}$, and *Trex1*$^{-/-}$*Irf3*$^{-/-}$ mice. (*C*) Real-time changes in the OCR of WT, *Trex1*$^{-/-}$, *Trex1*$^{-/-}$*Sting*$^{gt/gt}$, and *Trex1*$^{-/-}$*Irf3*$^{-/-}$ BMDMs. Data are representative of at least two independent experiments.

and mortality of *Trex1*$^{-/-}$ mice (Fig. 2 *A* and *B* and refs. 3 and 5). We next examined cellular metabolic phenotypes of *Trex1*$^{-/-}$*Sting*$^{gt/gt}$ and *Trex1*$^{-/-}$*Irf3*$^{-/-}$ cells. Surprisingly, we found that *Sting*$^{gt/gt}$ fully rescued the mitochondrial-respiration defect associated with *Trex1*$^{-/-}$, but *Irf3*$^{-/-}$ did not (Fig. 2*C*). These data suggest that mitochondrial-respiration defect persists in *Trex1*$^{-/-}$*Irf3*$^{-/-}$ cells, despite complete shutoff of IFN signaling and inflammation. Together, we conclude that mTORC1 is regulated by a STING-dependent, but IRF3-independent, mechanism in *Trex1*$^{-/-}$ mice. Our data also indicate that inflammation and metabolic defect in *Trex1*$^{-/-}$ mice can be genetically separated by *Irf3*$^{-/-}$.

Chronically Activated TBK1 Inhibits mTORC1 Activity. We next investigated the STING-dependent but IRF3-independent regulation of mTORC1 activity. One possibility is that STING recruits TBK1 to phosphorylate IRF3 and that chronically activated TBK1 may directly inhibit mTORC1. A previous study found that TBK1 interacts with mTORC1 and inhibits its activity in prostate cancer cells (12). In the case of DNA sensing, STING recruits TBK1 to form the "STING signalsome" as soon as it exits the ER, and both proteins travel through the secretory pathway, potentially reaching lysosomes where mTORC1 is located (13). To test this possibility, we first knocked down TBK1 in WT and *Trex1*$^{-/-}$ cells using four independent siRNAs. TBK1 knockdown in WT MEFs increased mTORC1 activity modestly above the already high steady-state level of mTORC1 activity (Fig. 3*A*; siRNA sequences are in Table S1). TBK1 knockdown in *Trex1*$^{-/-}$ MEFs clearly restored mTORC1 activity to WT level (Fig. 3*A*). We next examined whether TBK1 binds mTORC1 in *Trex1*$^{-/-}$ cells. We immunoprecipitated endogenous TBK1 from WT and *Trex1*$^{-/-}$ BMDMs and blotted for mTORC1 cofactors and substrates. Remarkably, we found that mTOR, Raptor, S6P, and 4EBP all coimmunoprecipitated with TBK1 only in *Trex1*$^{-/-}$ cells but not in WT cells (Fig. 3*B*). We next validated TBK1:mTOR interaction by overexpression of epitope tagged proteins and coimmunoprecipitation in 293T cells (Fig. 3*C*). Together, these data suggest that TBK1 inhibits mTORC1 activity through direct binding to the mTORC1 complex and that interaction is enhanced in *Trex1*$^{-/-}$ cells. Together with our genetic evidence, these data suggest that chronic activation of TBK1 promotes its interaction with mTORC1, resulting in inhibited mTORC1 activity in *Trex1*$^{-/-}$ cells.

***Trex1*$^{-/-}$ Mice Exhibit Systemic Metabolic Defect, Including Reduced Adiposity and Increased Energy Expenditure.** We next investigated whether the cellular metabolic defect caused by *Trex1*$^{-/-}$ is associated with any in vivo systemic metabolic phenotypes. Because mitochondrial respiration (oxidative phosphorylation) was reduced in *Trex1*$^{-/-}$ cells, it is possible that *Trex1*$^{-/-}$ mice use fat as an alternate source of energy and become hypermetabolic in vivo. Increased lipolysis has been reported in patients treated with an mTORC1 inhibitor, rapamycin, following organ transplantation (14). *S6K*$^{-/-}$ or Raptor conditional knockout mice also showed altered lipid metabolic profiles (8, 9). Indeed, we observed significant reduction of body fat in *Trex1*$^{-/-}$ mice compared with age-matched WT controls (Fig. 4*A*). To pinpoint exact location(s) where fat is reduced, we used high-resolution micro-computed tomography (CT) scan and found significant reduction of fat both in subcutaneous tissues and visceral tissues, as well as brown fat (Fig. 4*B*).

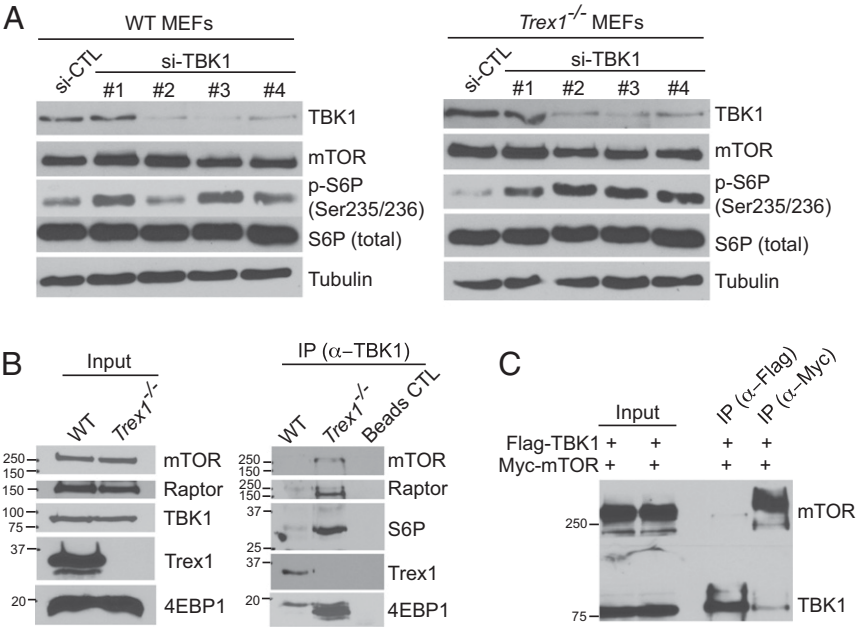

Fig. 3. TBK1 is recruited to the mTORC1 complex and inhibits mTORC1 complex activity in *Trex1*$^{-/-}$ cells. (*A*) Immunoblot analyses of mTORC1 activity in WT or *Trex1*$^{-/-}$ MEFs after control or TBK1 knocked down by siRNA. (*B*) Immunoblot analyses of TBK1–mTORC1 interaction in WT or *Trex1*$^{-/-}$ BMDMs. IP was performed with anti-TBK1 antibody and subsequently blotted for indicated proteins. (*C*) Immunoblot analyses of TBK1–mTORC1 interactions by transient transfection of Flag-TBK1 and Myc-mTOR plasmids and IP with indicated antibodies (*Upper*) in 293T cells. Both Flag-TBK1 and Myc-mTORC1 were expressed in both conditions, but Flag IP was performed in one sample and blot for Myc (upper strip of membrane), and Myc was performed in another sample and blot for Flag (lower strip of membrane).

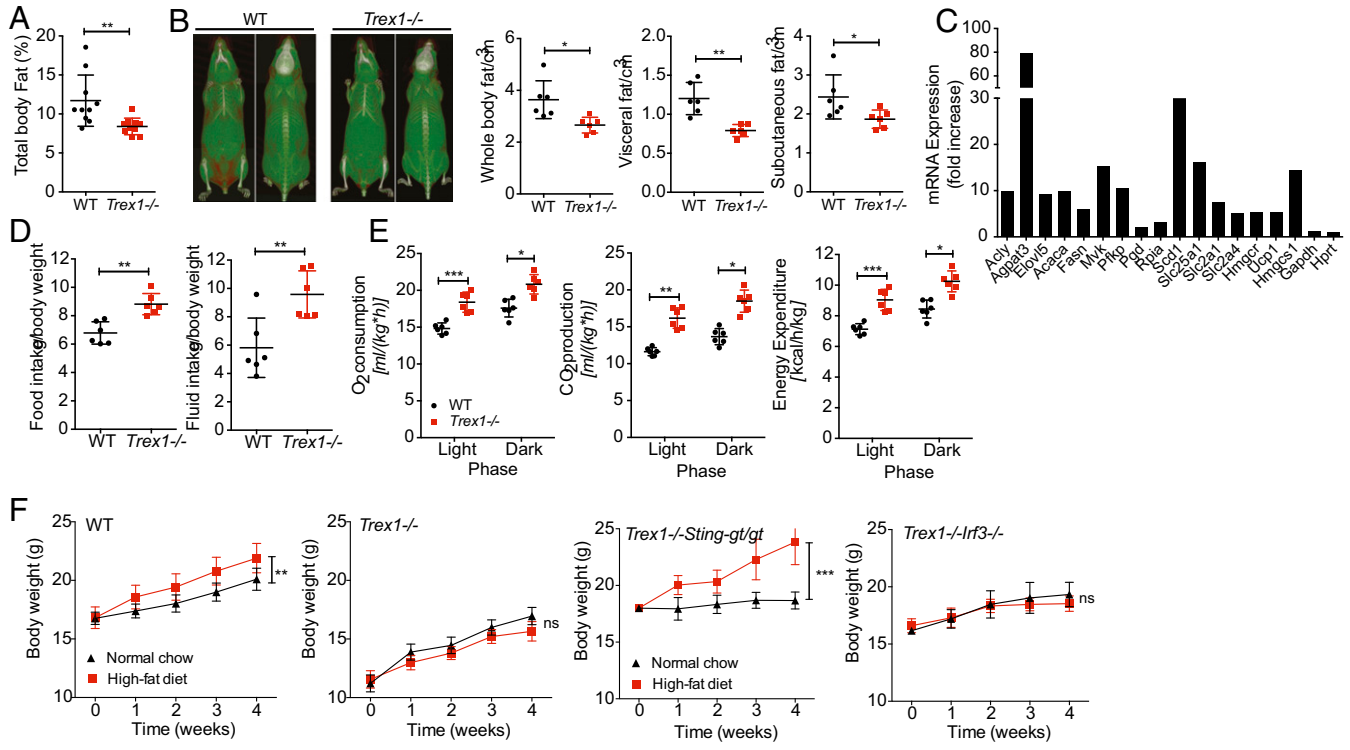

Fig. 4. *Trex1*$^{-/-}$ mice exhibit a hypermetabolic state with reduced adiposity and increased energy expenditure. (*A*) Percentage of total body fat in WT and *Trex1*$^{-/-}$ mice ($n = 10$). (*B*) High-resolution micro-CT scan images of WT and *Trex1*$^{-/-}$ mice (front and back view of the same mouse, red indicates fat mass). Representative images are shown on the left. Quantitation of whole-body, visceral, and subcutaneous fat volume is shown on the right ($n = 6$). (C) qRT-PCR analysis of selected genes involved in lipid metabolic pathways. (*D*) Food and fluid intake in WT and *Trex1*$^{-/-}$ mice over a period of 5 d ($n = 6$). (*E*) Oxygen consumption, CO_2 production, and energy expenditure in WT and *Trex1*$^{-/-}$ mice ($n = 6$). (*F*) Body weights of WT or *Trex1*$^{-/-}$, *Trex1*$^{-/-}$*Sting*$^{gt/gt}$, and *Trex1*$^{-/-}$*Irf3*$^{-/-}$ mice on normal chow or HFD over a period of 4 wk ($n = 9$). Data are presented as the means ± SEM $*P < 0.05$; $**P < 0.01$; $***P < 0.001$ (Student's *t* test).

We next performed lipid analysis in serum and did not observe any significant differences in nonesterified fatty acids (NEFAs), triglycerides, or cholesterols (Fig. S2 *A*–*C*). We also did not observe any differences in fatty acid oxidation (Fig. S2*D*). We also did not observe any difference in white adipose tissue (Fig. S2*E*). We next isolated brown adipose tissue from WT and *Trex1*$^{-/-}$ mice and measured the expression of several genes known to be involved in fat metabolism. Genes involved in fat metabolic pathways (15), such as *Agpat3*, *Scd1*, and many others, were highly up-regulated (5–80-fold) in *Trex1*$^{-/-}$ brown adipose tissue compared with WT (Fig. 4*C*), consistent with accelerated fat metabolism.

We also monitored bioenergetics profiles of WT and *Trex1*$^{-/-}$ mice using metabolic cage. We observed increased food and fluid intake (Fig. 4*D*), as well as significant increase in oxygen consumption, carbon dioxide production, and heat production in *Trex1*$^{-/-}$ mice (Fig. 4*E*). To further characterize the hypermetabolic phenotype and determine whether this in vivo phenotype also depends on STING or IRF3, we challenged WT, *Trex1*$^{-/-}$, *Trex1*$^{-/-}$*Sting*$^{gt/gt}$, and *Trex1*$^{-/-}$*Irf3*$^{-/-}$ mice with a high-fat diet (HFD) over a period of 4 wk (median survival of *Trex1*$^{-/-}$ mice is around 8–10 wk). We found that *Trex1*$^{-/-}$ and *Trex1*$^{-/-}$*Irf3*$^{-/-}$ mice did not gain any additional weight during the HFD challenge, whereas WT and *Trex1*$^{-/-}$*Sting*$^{gt/gt}$ mice gained significantly more weight during the same period on HFD (Fig. 4*F*). These data demonstrate that the in vivo hypermetabolic phenotype observed in *Trex1*$^{-/-}$ mice is also STING-dependent and IRF3-independent, which implies that the reduced cellular mitochondrial respiration and increased in vivo fat metabolism are likely associated, and both could be caused by chronically suppressed mTORC1 activity.

We next crossed *Trex1*$^{-/-}$ mice to *Leptin*-deficient (*Ob*/*Ob*) mice to determine whether we can genetically rescue the hypermetabolic phenotype of *Trex1*$^{-/-}$ mice by enhancing lipogenesis. Remarkably, *Trex1*$^{-/-}$*Ob*/*Ob* mice restored body weight to that of WT and heterozygous littermate controls, all significantly lower compared with littermate *Ob*/*Ob* mice (Fig. 5*A*). Inflammatory cytokines such as IL-6 and TNFα remain elevated in *Trex1*$^{-/-}$*Ob*/*Ob* mice compared with WT mice, at levels similar to *Trex1*$^{-/-}$ mice, suggesting that *Ob*/*Ob* did not dampen inflammation (Fig. 5*B*). This observation further supports the notion that inflammation and metabolism can be genetically separated. *Trex1*$^{-/-}$*Ob*/*Ob* mice were able to exceed WT in body weight after 3 mo of age, while still weighing less than *Ob*/*Ob* mice (Fig. 5*C*). CT scans also showed less body fat in *Trex1*$^{-/-}$*Ob*/*Ob* mice compared with *Trex1*$^{+/+}$*Ob*/*Ob* mice (Fig. 5*D*). More importantly, we observed significant increase in survival of *Trex1*$^{-/-}$*Ob*/*Ob* mice compared with *Trex1*$^{-/-}$ alone (Fig. 5*E*). Although systemic inflammation is the predominant cause of mortality in *Trex1*$^{-/-}$ mice, our data showed that enhancing lipogenesis can prolong the survival of *Trex1*$^{-/-}$ mice without dampening inflammation, suggesting that the hypermetabolic phenotype, likely a consequence of reduced mTORC1 activity, is an important contributing factor to the overall morbidity of *Trex1*$^{-/-}$ mice.

***Trex1*$^{-/-}$ Mice Support Accelerated Growth of Implanted Breast Cancer Cells.** Persistent mTORC1 inhibition by rapalogs (analogs of rapamycin) has been reported to cause liver damage, inflammation, and enhanced tumorigenesis (16). The reduced mitochondrial respiration and increased glycolysis of *Trex1*$^{-/-}$ cells also resembles the Warburg effect (17), although spontaneous tumor has not been observed in *Trex1*$^{-/-}$ mice during their short lifespan. We next examined whether *Trex1*$^{-/-}$ mice could alter the growth rate of implanted cancer cells. We implanted E0771 breast cancer cells [derived from breast tumor in a C57BL/6 mouse (18)] in the mammary pad of WT and *Trex1*$^{-/-}$ mice and followed the mice over a period of 3–4 wk. Remarkably, *Trex1*$^{-/-}$ mice supported two- to threefold increase in primary tumor size and more frequent lung metastasis compared with age-matched WT mice (Fig. 6 *A*

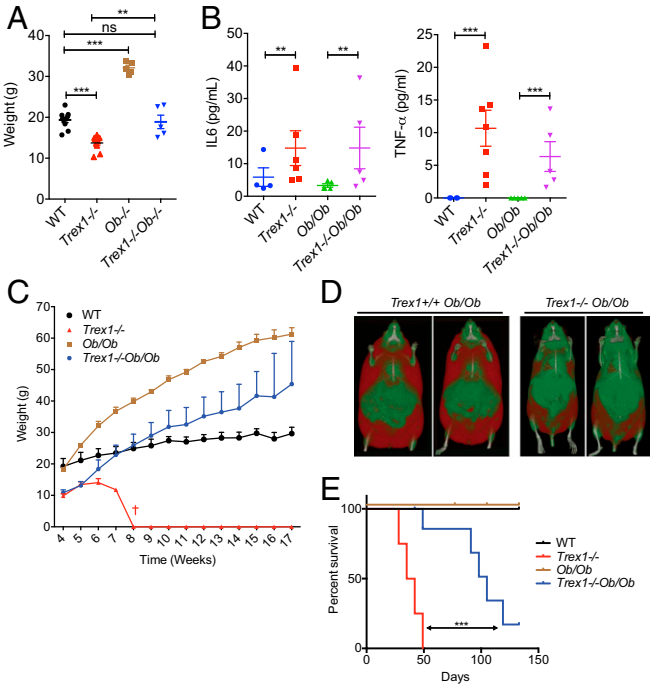

Fig. 5. *Leptin* deficiency (*Ob/Ob*) increases lipogenesis and survival of *Trex1*$^{-/-}$ mice without dampening inflammation. (*A*) Body weights of mice of indicated genotypes on normal chow diet for 6 wk (n = 5–10). (*B*) Serum levels of indicated inflammatory cytokines. (*C*) Body weights of mice of indicated genotypes on normal chow diet for a period 17 wk (n = 5–10). (*D*) High-resolution micro-CT scan images of WT and *Trex1*$^{-/-}$ mice on *Ob/Ob* background (front view of two separate mice, red indicates fat mass). (*E*) Survival curve of mice of indicated genotypes (n = 5–10). Data are presented as the means ± SEM. *P < 0.05; **P < 0.01; ***P < 0.001. (*A* and *B*, Student's t test; *E*, log-rank test.)

and *B*). To determine whether STING- or IRF3-mediated signaling is also playing a role, we performed similar xenograft experiments in *Trex1*$^{-/-}$*Sting*$^{gt/gt}$ and *Trex1*$^{-/-}$*Irf3*$^{-/-}$ mice. We found that *Trex1*$^{-/-}$*Irf3*$^{-/-}$ mice also supported increased tumor growth, whereas *Trex1*$^{-/-}$*Sting*$^{gt/gt}$ mice are indistinguishable to WT mice in tumor growth (Fig. 6*C*). These data provide yet another line of evidence for an IRF3-independent STING-signaling branch in *Trex1*$^{-/-}$ mice, which could create a favorable microenvironment or immune status that enhances tumorigenesis (for a model, see Fig. 7).

Discussion

We present here an autoimmune/autoinflammatory disease mouse model, *Trex1*$^{-/-}$, with evidence of cellular and systemic metabolic dysregulation and chronically suppressed mTORC1 activity. TREX1 is best known for its DNase activity, which prevents sensing of cytosolic self-DNA by the cGAS–STING pathway and activation of the IFN response (6, 7). The striking resemblance of *Trex1*$^{-/-}$ mice's lean appearance to the phenotypes of S6K- or Raptor-deficient mice (8, 9), together with significantly reduced mTORC1 activity in tissues, provided a strong clue that chronic activation of immune pathways in *Trex1*$^{-/-}$ mice may play an important role in mTORC1 regulation and metabolism. We provide evidence that inflammation and metabolic defects in *Trex1*$^{-/-}$ mice can be genetically separated. Both *Trex1*$^{-/-}$*Sting*$^{gt/gt}$ and *Trex1*$^{-/-}$*Irf3*$^{-/-}$ mice fully rescued mortality and inflammation caused by *Trex1*$^{-/-}$. Importantly, *Trex1*$^{-/-}$*Sting*$^{gt/gt}$ also rescued the cellular mitochondrial respiration and systemic hypermetabolic phenotypes associated with *Trex1*$^{-/-}$, whereas *Trex1*$^{-/-}$*Irf3*$^{-/-}$ failed to rescue either metabolic phenotype. Complementing these findings are the genetic crosses to *Ob/Ob* mice, where *Trex1*$^{-/-}$*Ob/Ob* mice increased lipogenesis and overall survival without dampening inflammation compared with *Trex1*$^{-/-}$ mice.

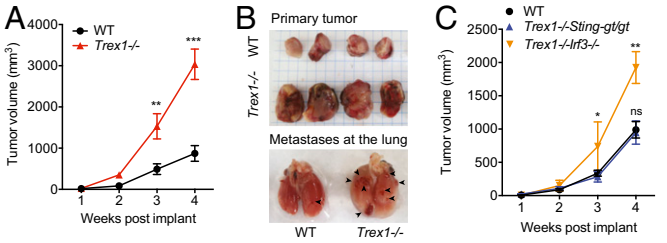

Fig. 6. *Trex1*$^{-/-}$ mice support accelerated growth of implanted breast cancer cells. (*A*) E0771 breast tumor growth in WT and *Trex1*$^{-/-}$ mice; 5 × 10^5 E0771 cells were injected into mammary pads of female WT and *Trex1*$^{-/-}$ mice. Tumor sizes were recorded weekly (n = 9). (*B*) Representative images of primary and metastatic tumor at week 4 from WT or *Trex1*$^{-/-}$ mice. (*C*) E0771 breast tumor growth in WT and *Trex1*$^{-/-}$*Sting*$^{gt/gt}$ and *Trex1*$^{-/-}$*Irf3*$^{-/-}$ mice. E0771 cells were injected as in *A*. Data are presented as the means ± SEM. *P < 0.05; **P < 0.01; ***P < 0.001; ns, not significant (Student's t test).

The key protein connecting STING and IRF3 is TBK1. TBK1 is a member of the IκB kinase family and is ubiquitously expressed. In addition to its role in innate immunity, TBK1 also plays an important role in cell proliferation and cancer (19), and *Tbk1* deficiency is embryonic-lethal. TBK1 has been shown to inhibit mTORC1 activity in prostate cancer cells (12, 20). T cell-specific ablation of TBK1 also enhances mTORC1 signaling in an experimental autoimmune encephalomyelitis model (20). We recently showed that pharmacological inhibition of TBK1 ameliorates disease phenotypes in *Trex1*$^{-/-}$ mice (21). STING activation involves trafficking from the ER to cytoplasmic vesicles through the secretory pathway (13), during which time TBK1 is recruited and travels with STING as part of the STING signalsome, which is potentially targeted to lysosomes for degradation to prevent excessive IFN response (22) (see the model in Fig. 7). mTORC1 localizes to the lysosomes, and we showed that *Trex1* deficiency enhances lysosome biogenesis through suppressing mTORC1 activity (1). We now further show with biochemical evidence that

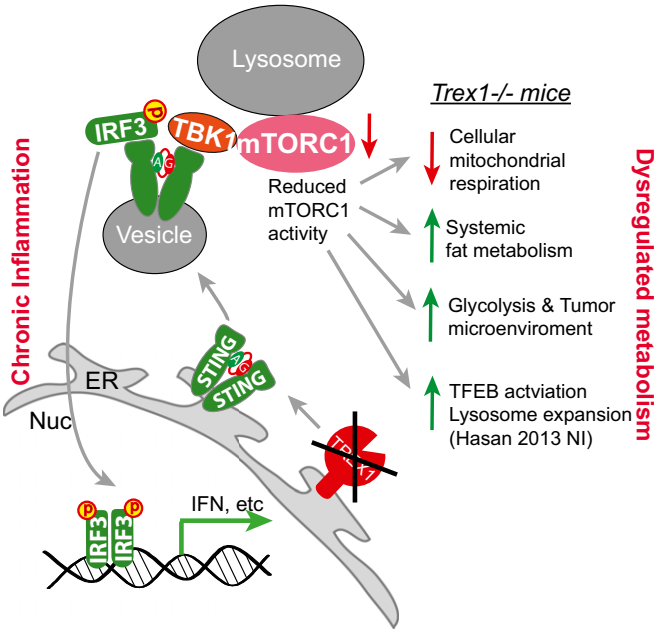

Fig. 7. A model. *Trex1*$^{-/-}$ leads to chronic activation of the STING–TBK1–IRF3 signaling pathway, leading to inflammation through IRF3 and mTORC1 inhibition by TBK1. Reduced mTORC1 activity causes metabolic dysregulation, including reduced mitochondrial respiration and increased glycolysis and fat metabolism.

TBK1 is recruited to the mTORC1 complex in *Trex1*$^{-/-}$ cells, and TBK1 knockdown by siRNA alleviated mTORC1 suppression in *Trex1*$^{-/-}$ cells. These molecular findings establish a plausible mechanism by which chronic STING activation and trafficking not only recruit TBK1 for IRF3 signaling but also bring TBK1 to close proximity with mTORC1 on the lysosomes. Consistent with this finding, mTORC1 substrate S6K was recently shown to be recruited to the STING–TBK1 complex to promote IFN signaling during acute DNA stimulation (23). The molecular details of the interaction between the STING signalsome and the mTORC1 complex, as well as functional consequences during acute and chronic DNA stimulation, require further investigation.

Trex1 deficiency leads to reduced mTORC1 activity in mouse cells and tissues, as well as impaired cellular metabolism (reduced mitochondrial respiration) and a hypermetabolic state (increased fat metabolism and glycolysis) in vivo. Both the cellular and systemic metabolic phenotypes are STING-dependent and IRF3-independent, and both phenotypes have previously being shown to be associated with reduced mTORC1, a master regulator of metabolism (8–10). The "cause" of inflammation (and innate immune signaling) in *Trex1*$^{-/-}$ mice has been clearly demonstrated by multiple groups to be the self-DNA-mediated activation of the cGAS–STING–TBK1–IRF3 pathway. In the context of this knowledge, decreased mTORC1 activity is the "consequence," not the cause, of *Trex1*-deficiency-mediated innate immune signaling; this decreased mTORC1 activity occurs cell-intrinsically. However, our study does not exclude the possibility of decreased mTORC1 in turn influencing overall inflammation. We also found that *Trex1* deficiency enhances growth of xenografted tumor, and this protumor effect is also STING-dependent but IRF3-independent. Whether this protumor effect is the result of chronic mTORC1 inhibition by TBK1 or the dysregulated host metabolism seen in *Trex1*$^{-/-}$ mice requires more investigation. Other host immune signaling downstream of STING, such as NF-κB or STAT6 activation (24), could also contribute to the overall protumor effect.

Together, we envision a model where chronic autoimmune activation of the STING–TBK1 pathway leads to reduced mTORC1 activity, which then causes dysregulated cellular and systemic metabolic phenotypes. We identify TBK1 as the critical factor that regulates both immune signaling (that leads to inflammation) and metabolism (through inhibiting mTORC1). Future studies are needed to further illuminate how TBK1 balances both activities in normal and in autoimmune disease settings. It will be interesting to investigate whether other chronic innate immune activation mouse models present similar metabolic phenotypes. Nonetheless, because metabolic dysregulation is becoming more commonly observed in autoimmune diseases such as SLE, which is often associated with elevated type I IFN gene signature and chronic activation of TBK1-dependent innate immune pathways (21, 25, 26). The molecular mechanism we delineated here with the *Trex1*$^{-/-}$ mouse model highlight TBK1 as a potentially useful therapeutic target that mediates the crosstalk between immune response and metabolism.

Materials and Methods

Cells, Mice, and Reagents. All animal experimental protocols were approved by the Institutional Animal Care and Use Committee of University of Texas Southwestern Medical Center at Dallas. *Trex1*$^{-/-}$ mice were described previously (1). *Trex1*$^{-/-}$*Ob/Ob* mice were generated by crossing *Trex1*$^{+/-}$ mice with *Ob/Ob* mice. All mice used in this study were from a C57BL/6 background, and experiments were conducted using littermate-controlled male or female mice. A detailed reagent list is in *SI Materials and Methods*.

RNA Isolation, Quantitative RT-PCR Analysis, Cytokine-Detection Assay, Western Blot, and Immunoprecipitation. RNA isolation and quantitative (q)RT-PCR analysis were performed as described previously (1). Serum cytokines were measured by MILLIPLEX multiplex assay using Luminex (EMD Millipore) according to the manufacturer's protocols. Western blots were performed as described previously (1). Coimmunoprecipitation experiments were performed as described previously (2).

Body Composition Analysis, Computed Topography, Metabolism Assay, and Tumor Study. A Whole Body Composition Analyzer (Bruker Minispec mq10; Bruker) was used to quantify total body fat, lean body mass, and fluid contents. For real-time analysis of the ECAR and OCR, cells were analyzed with XF-24-3 extracellular flux analyzer (Seahorse Bioscience) according to the manufacturer's recommendations. Serum NEFA measurements were done using the Vitros 250 Chemistry System at the University of Texas Southwestern Medical Center Mouse Metabolic and Phenotyping Core. For more detailed information, see *SI Materials and Methods*.

ACKNOWLEDGMENTS. We thank Beth Levine (University of Texas Southwestern Medical Center) for the E0771 cells and expression plasmids for mTOR and TBK1, Philipp Scherer (University of Texas Southwestern Medical Center) for *Ob/Ob* mice, Min Ae Lee-Kirsch (Technische Universität Dresden) for TREX1 patient cells, and Charles Fermaintt for technical assistance. We also thank members of the N.Y. laboratory for helpful discussions. This work was supported by US National Institutes of Health Grants AI098569 and AR067135 (to N.Y.), the Alliance for Lupus Foundation (N.Y.), and Welch Foundation Grant I-1831 (to N.Y.).

1. Hasan M, et al. (2013) Trex1 regulates lysosomal biogenesis and interferon-independent activation of antiviral genes. *Nat Immunol* 14(1):61–71.
2. Hasan M, et al. (2015) Cytosolic nuclease TREX1 regulates oligosaccharyltransferase activity independent of nuclease activity to suppress immune activation. *Immunity* 43(3):463–474.
3. Stetson DB, Ko JS, Heidmann T, Medzhitov R (2008) Trex1 prevents cell-intrinsic initiation of autoimmunity. *Cell* 134(4):587–598.
4. Crow YJ, Rehwinkel J (2009) Aicardi-Goutieres syndrome and related phenotypes: linking nucleic acid metabolism with autoimmunity. *Hum Mol Genet* 18(R2):R130–R136.
5. Gall A, et al. (2012) Autoimmunity initiates in nonhematopoietic cells and progresses via lymphocytes in an interferon-dependent autoimmune disease. *Immunity* 36(1):120–131.
6. Gao D, et al. (2015) Activation of cyclic GMP-AMP synthase by self-DNA causes autoimmune diseases. *Proc Natl Acad Sci USA* 112(42):E5699–E5705.
7. Gray EE, Treuting PM, Woodward JJ, Stetson DB (2015) Cutting edge: cGAS is required for lethal autoimmune disease in the Trex1-deficient mouse model of Aicardi-Goutières syndrome. *J Immunol* 195(5):1939–1943.
8. Polak P, et al. (2008) Adipose-specific knockout of raptor results in lean mice with enhanced mitochondrial respiration. *Cell Metab* 8(5):399–410.
9. Um SH, et al. (2004) Absence of S6K1 protects against age- and diet-induced obesity while enhancing insulin sensitivity. *Nature* 431(7005):200–205.
10. Chen Z, et al. (2014) Mutation of mouse Samd4 causes leanness, myopathy, uncoupled mitochondrial respiration, and dysregulated mTORC1 signaling. *Proc Natl Acad Sci USA* 111(20):7367–7372.
11. Cheng T, et al. (2011) Pyruvate carboxylase is required for glutamine-independent growth of tumor cells. *Proc Natl Acad Sci USA* 108(21):8674–8679.
12. Kim JK, et al. (2013) TBK1 regulates prostate cancer dormancy through mTOR inhibition. *Neoplasia* 15(9):1064–1074.
13. Dobbs N, et al. (2015) STING activation by translocation from the ER is associated with infection and autoinflammatory disease. *Cell Host Microbe* 18(2):157–168.
14. Pereira MJ, et al. (2013) The immunosuppressive agents rapamycin, cyclosporin A and tacrolimus increase lipolysis, inhibit lipid storage and alter expression of genes involved in lipid metabolism in human adipose tissue. *Mol Cell Endocrinol* 365(2):260–269.
15. Düvel K, et al. (2010) Activation of a metabolic gene regulatory network downstream of mTOR complex 1. *Mol Cell* 39(2):171–183.
16. Umemura A, et al. (2014) Liver damage, inflammation, and enhanced tumorigenesis after persistent mTORC1 inhibition. *Cell Metab* 20(1):133–144.
17. Vander Heiden MG, Cantley LC, Thompson CB (2009) Understanding the Warburg effect: the metabolic requirements of cell proliferation. *Science* 324(5930):1029–1033.
18. Ewens A, Mihich E, Ehrke MJ (2005) Distant metastasis from subcutaneously grown E0771 medullary breast adenocarcinoma. *Anticancer Res* 25(6B):3905–3915.
19. Ou Y-H, et al. (2011) TBK1 directly engages Akt/PKB survival signaling to support oncogenic transformation. *Mol Cell* 41(4):458–470.
20. Yu J, et al. (2015) Regulation of T-cell activation and migration by the kinase TBK1 during neuroinflammation. *Nat Commun* 6:6074.
21. Hasan M, et al. (2015) Cutting edge: inhibiting TBK1 by compound II ameliorates autoimmune disease in mice. *J Immunol* 195(10):4573–7.
22. Konno H, Konno K, Barber GN (2013) Cyclic dinucleotides trigger ULK1 (ATG1) phosphorylation of STING to prevent sustained innate immune signaling. *Cell* 155(3):688–698.
23. Wang F, et al. (2016) S6K-STING interaction regulates cytosolic DNA-mediated activation of the transcription factor IRF3. *Nat Immunol* 17(5):514–522.
24. Chen H, et al. (2011) Activation of STAT6 by STING is critical for antiviral innate immunity. *Cell* 147(2):436–446.
25. Bennett L, et al. (2003) Interferon and granulopoiesis signatures in systemic lupus erythematosus blood. *J Exp Med* 197(6):711–723.
26. Becker AM, et al. (2013) SLE peripheral blood B cell, T cell and myeloid cell transcriptomes display unique profiles and each subset contributes to the interferon signature. *PLoS One* 8(6):e67003.